Autophagy machinery promotes the chaperone-mediated formation and compartmentalization of protein aggregates during appressorium development by the rice blast fungus

Audra Mae Rogers[a] and Martin John Egan[a,b,*]
[a]Department of Entomology and Plant Pathology, Division of Agriculture, University of Arkansas Systems, Fayetteville, AR 72701; [b]Cell and Molecular Biology Program, University of Arkansas, Fayetteville, AR 72701

ABSTRACT **The chaperone-mediated sequestration of misfolded proteins into specialized quality control compartments represents an important strategy for maintaining protein homeostasis in response to stress. However, precisely how this process is controlled in time and subcellular space and integrated with the cell's protein refolding and degradation pathways remains unclear. We set out to understand how aggregated proteins are managed during infection-related development by a globally devastating plant pathogenic fungus and to determine how impaired protein quality control impacts cellular differentiation and pathogenesis in this system. Here we show that in the absence of Hsp104 disaggregase activity, aggregated proteins are spatially sequestered into quality control compartments within conidia, but not within terminally differentiated infection cells, and thus spatial protein quality control is cell type–dependent. We demonstrate that impaired aggregate resolution results in a short-term developmental penalty but has no significant impact upon appressorium function. Finally, we show that, somewhat unexpectedly, the autophagy machinery is necessary for the normal formation and compartmentalization of protein aggregates. Taken together, our findings provide important new insight into spatial protein quality control during the process of terminal cellular differentiation by a globally important model eukaryote and reveal a new level of interplay between major proteostasis pathways.**

Monitoring Editor
Karsten Weis
ETH Zurich

Received: Jan 27, 2020
Revised: Jul 14, 2020
Accepted: Aug 3, 2020

INTRODUCTION

The fungus *Magnaporthe oryzae* breaks into and parasitizes the foliar tissue of susceptible rice plants, resulting in a devastating disease called blast, which destroys enough rice annually to feed 60 million people for 1 yr (Skamnioti and Gurr, 2009). Infections begin when a three-celled spore called a conidium lands on the surface of a rice leaf. In the presence of free water, the conidium initiates a complex morphogenetic program culminating in the formation of a specialized infection cell called an appressorium (Wilson and Talbot, 2009; Figure 1A). Development of a functional appressorium requires the autophagic recycling of conidial cell contents, which are subsequently trafficked into the developing appressorium, resulting in collapse and death of the conidium (Veneault-Fourrey *et al.*, 2006; Kershaw and Talbot, 2009). Appressoria mechanically rupture the otherwise impenetrable leaf cuticle through the directed application of enormous hydrostatic turgor pressure, which builds within these melanized cells (Howard *et al.*, 1991; Figure 1A), allowing the fungus to enter and colonize host tissue. During the establishment of disease, microbial pathogens like *M. oryzae* are exposed to diverse cellular stressors, which can cause damage to their proteome and the formation of toxic misfolded protein conformers. An important and broadly conserved

This article was published online ahead of print in MBoC in Press (http://www.molbiolcell.org/cgi/doi/10.1091/mbc.E20-01-0068) on August 20, 2020.
Competing interests: The authors declare no competing financial interests.
*Address correspondence to: Martin John Egan (me021@uark.edu).
Abbreviations used: ANOVA, analysis of variance; CM, complete media; CTAB, cetyl trimethyl ammonium bromide; DWB, Double Walker B; GFP, green fluorescent protein TagGFP2; hpi, hours postinoculation; RFP, red fluorescent protein.

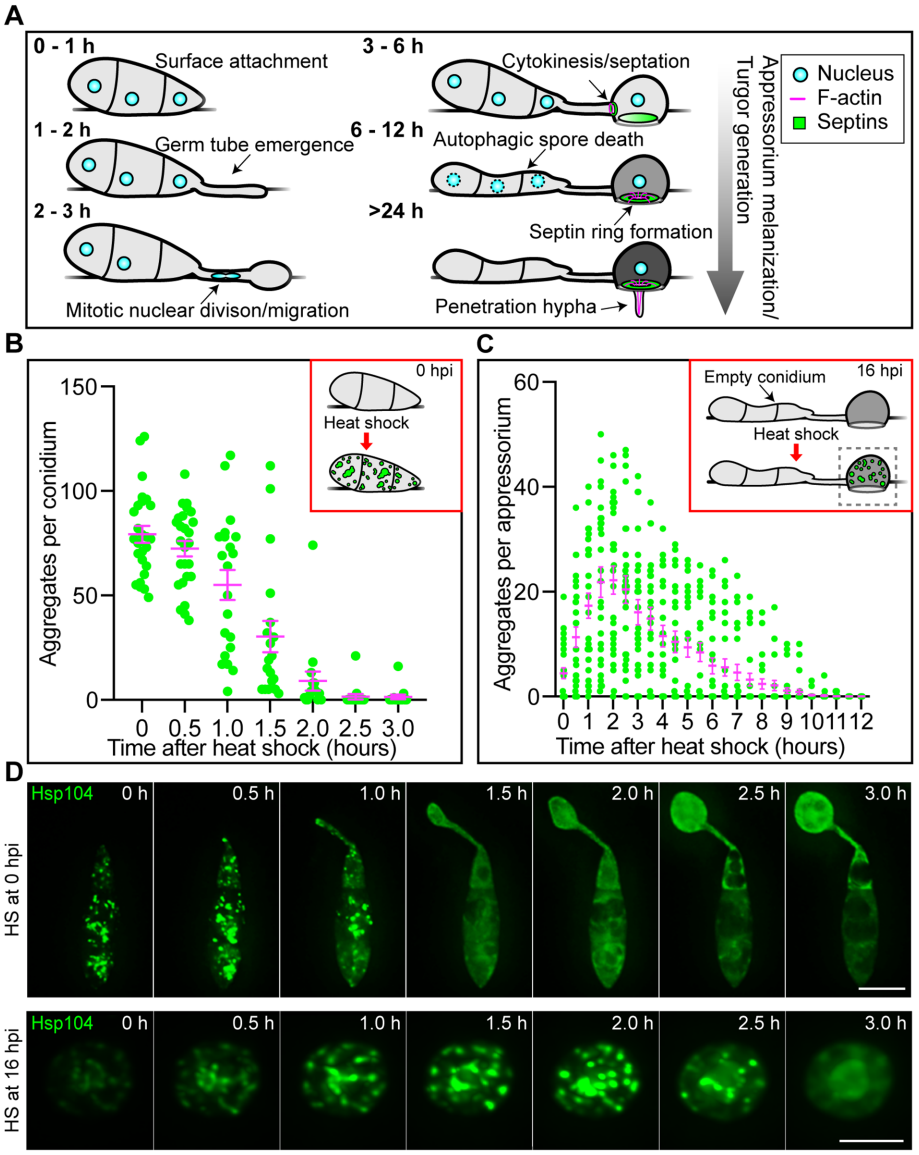

FIGURE 1: Hsp104-positive protein aggregates are cleared during infection-related development. (A) Cartoon depicting relevant morphogenetic landmarks associated with appressorium development by *M. oryzae*, based on previous observations (Veneault-Fourrey *et al.*, 2006; Saunders *et al.*, 2010b; Dagdas *et al.*, 2012; Dulal *et al.*, 2020). (B, C) Plots showing a time course of the number of Hsp104-positive aggregates present in conidia (B), and fully mature appressoria (C), following recovery from heat shock. Red-boxed schematics indicate at which time point heat shock was applied. Green circles represent individual conidia or appressoria. Magenta lines show the mean ± SEM. (D) Time-lapse sequences showing the localization of Hsp104-GFP–labeled protein aggregates following the exposure of ungerminated conidia (top panels) and fully mature appressoria (bottom panels) to heat shock. Scale bar = 5 µm. All images represent maximum-intensity projections of Z series acquired at 0.2 µm intervals spanning the depth of the cells.

been explored in the context of terminally differentiated cell types. We were curious as to how aggregated proteins are spatially and temporally managed during infection-related morphogenesis by the rice blast fungus and how dysfunction in protein quality control mechanisms impacts cellular differentiation and pathogenesis in this system. Appressorium development by *M. oryzae* proceeds to completion on artificial substrates, making it a compelling system to understand the principles of spatial protein quality control during the formation of terminally differentiated cell types.

RESULTS AND DISCUSSION

To observe aggregated proteins in *M. oryzae*, we generated a strain in which the molecular disaggregase Hsp104, an established marker for protein aggregates (Kaganovich *et al.*, 2008), was genetically tagged with the green fluorescent protein TagGFP2 (Subach *et al.*, 2008) (referred to herein as GFP). To induce proteostatic stress, we heat shocked conidia (42°C for 45 min) immediately after their adherence to cover glass. Hsp104-positive aggregates formed within each of the three cells of the conidia and resolved over the course of 3 h (Figure 1, B and D, top panel). In the absence of heat shock, Hsp104-positive aggregates were not detected at any time point during appressorium formation in vitro (Supplemental Figure S1A). Of course, this might not be the case for conidia germinating on the comparatively hostile rice leaf surface, where they likely encounter a barrage of stressors including oxidative assault from host cells (Wojtaszek, 1997). We wondered how protein aggregates are managed in mature appressoria, which would normally be primed for plant invasion, and therefore heat-shocked appressoria that had fully formed on cover glass (16 hours postinoculation [hpi]), and we observed the behavior of protein aggregates in this specialized cell type. Hsp104-positive protein aggregates were slower to form in differentiated appressoria than in conidia and persisted longer before ultimately resolving (Figure 1, C and D, bottom panel). Interestingly, protein stability and refolding behavior within the mature appressorium is likely modulated by the enormous osmotic turgor pressure that builds within this cell type, reaching up to 8.0 MPa (~80 atmospheres; Howard *et al.*, 1991; Chen and Makhatadze, 2017). The generation of osmolytes, including glycerol, which accumulate to molar concentrations within the appressorium, may contribute to protein stabilization during turgor production (de Jong *et al.*, 1997; Street *et al.*, 2006). Thus, we speculate that the differential behavior of protein aggregates within conidial cells and appressoria is likely due to the unique biochemical and biophysical properties of the appressorium.

strategy for managing damaged proteins in eukaryotes is to direct them to specialized inclusion bodies, or quality control compartments, where they can be processed later by the cell (Sontag *et al.*, 2017). This process, often referred to as spatial protein quality control, operates, for example, during cell division and serves to promote the integrity of daughter cells through the asymmetric retention of damaged proteins and aging determinants in the mother cell (Spokoini *et al.*, 2012; Ogrodnik *et al.*, 2014). Precisely how these quality control compartments form, and are ultimately processed by the cell, remains an active area of research and has not

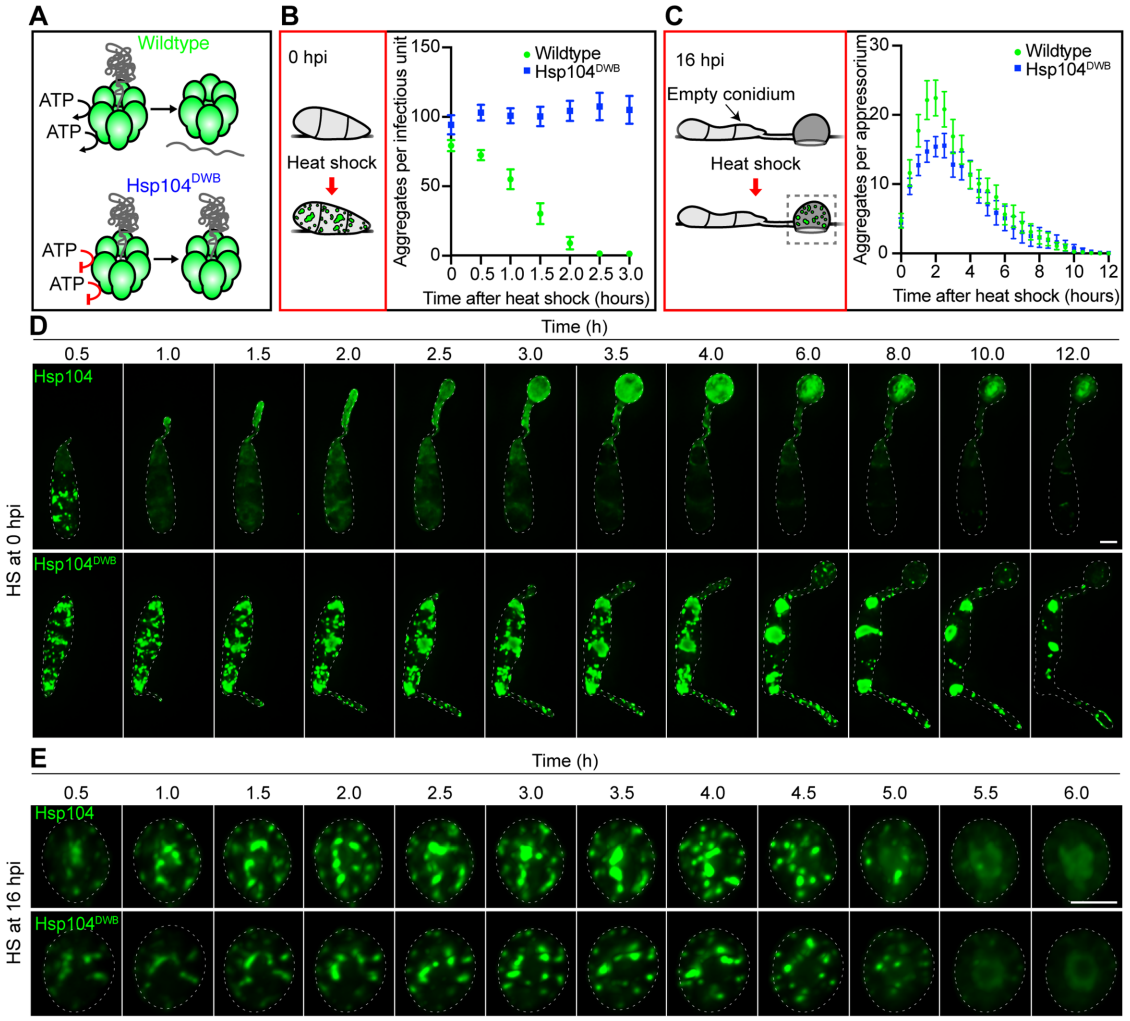

FIGURE 2: Protein aggregates are directed to quality control compartments in the absence of normal Hsp104 disaggregase activity. (A) Cartoon depicting blocked ATP hydrolysis and impaired disaggregase activity, but not substrate binding, by Hsp104 following the introduction of mutations in the two Walker B motifs within the nucleotide-binding sites (Hsp104^{DWB}). (B, C) Plots showing the mean number (± SEM) of Hsp104-positive aggregates in wild type vs. Hsp104^{DWB} mutants following recovery from heat shock. (B) For wild type, n >14 conidia per time point, and for Hsp104^{DWB}, n >19 conidia per time point. Red-boxed schematics indicate at which time point heat shock was applied. (C) Number of Hsp104-positive aggregates in appressoria heat shocked after 16 h of development. For wild type, n = 27 and for the Hsp104^{DWB} mutant, n = 34 at time point. (D, E) Time-lapse sequences showing the localization of Hsp104-GFP–labeled (top panels) and Hsp104^{DWB}-GFP–labeled (bottom panel) protein aggregates following the exposure of conidia (D) or appressoria (E) to heat shock. Scale bar = 5 µm. All images represent maximum-intensity projections of Z series acquired at 0.2 µm intervals spanning the depth of the cells.

An important and broadly conserved consequence of spatial protein quality control in eukaryotes is the asymmetric retention of damaged proteins, organelles, and aging determinants within mother cells, which is thought to impart a fitness advantage on daughter cells (Aguilaniu *et al.*, 2003; Zhou *et al.*, 2011; Spokoini *et al.*, 2012; Ogrodnik *et al.*, 2014; Sontag *et al.*, 2017). In the context of rice blast disease, maintaining the proteostatic integrity of the appressorium would seem imperative, since appressorium function is essential for establishing plant infection. We therefore wondered whether misfolded proteins would be actively retained within the conidium during appressorium development, thereby promoting the fitness of the infection cell prior to plant invasion. To test this idea, we generated an Hsp104 Double Walker B mutant (Hsp104^{DWB}) that can bind to misfolded proteins but not disaggregate them (Hodson *et al.*, 2012; Figure 2A). Our Hsp104^{DWB} mutant produced a number of protein aggregates comparableto that of the wild-type strain following heat shock (Figure 2, B and E). However, rather than resolving over the course of several hours, Hsp104^{DWB}-GFP–positive puncta persisted in the conidium, coalescing into large quality control compartments (Figure 2D, bottom panels). In striking contrast, the beha vior of protein aggregates in fully formed appressoria of the Hsp104^{DWB} mutant was largely indistinguishable from that of the wild type (Figure 2, C and E), and there was no major coalescence of protein aggregates into a central quality control compartment as seen in conidial cells (Figure 2, D, bottom panels vs. E, bottom panels). Thus, aggregated proteins are spatially and temporally managed in a cell type–dependent manner during infectious development by the rice blast fungus.

Despite the coalescence of protein aggregates into quality control compartments within the conidia of Hsp104^{DWB} mutants, a

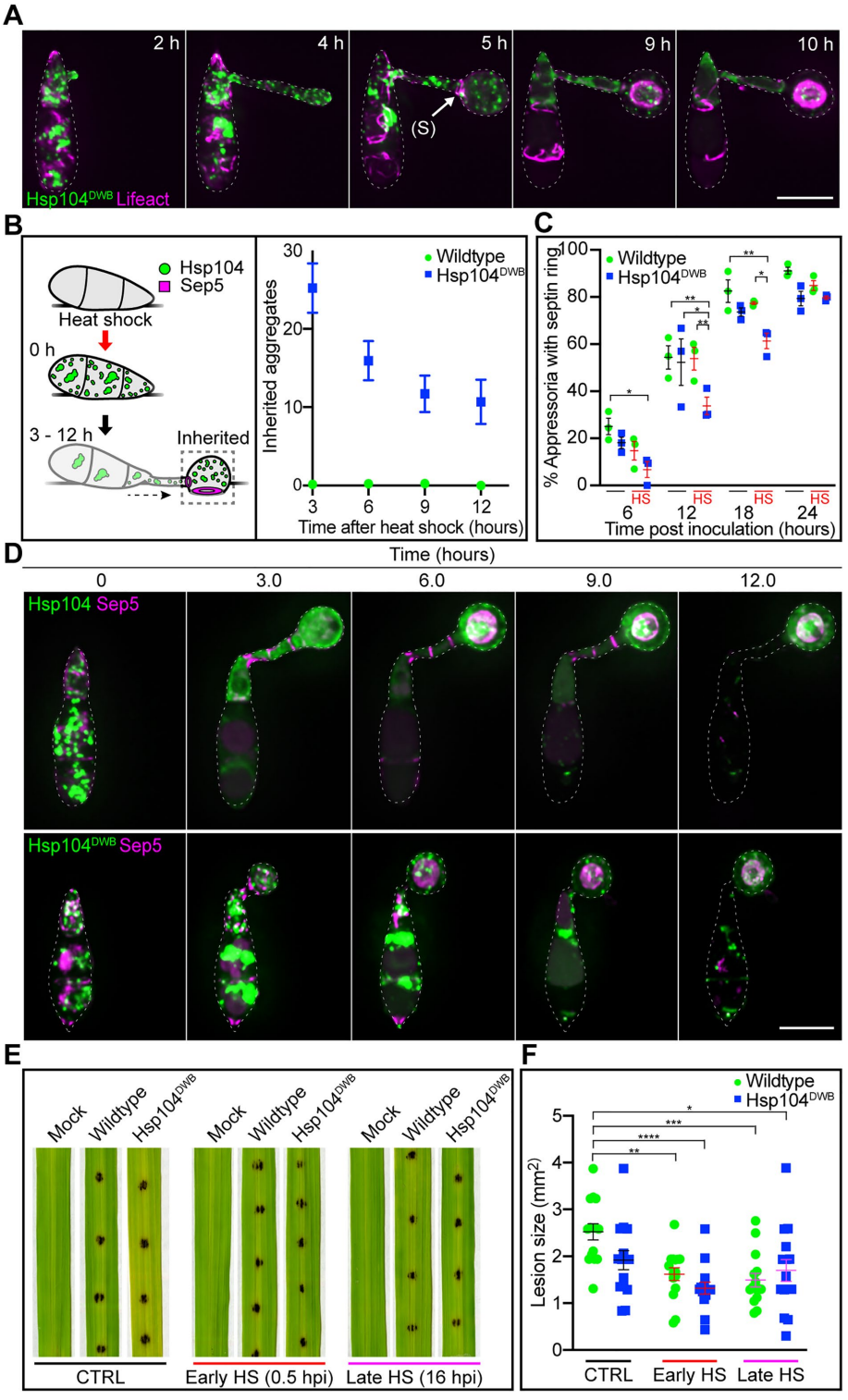

FIGURE 3: Impaired aggregate clearance delays infection-related development. (A) Time-lapse sequence showing a heat-shocked conidium coexpressing Hsp104^{DWB}-GFP and Lifeact-RFP. White arrow highlights a Lifeact-RFP–labeled cytokinetic ring demarking a site of septation (S) at the neck of the appressorium. (B) Cartoon depicting the approach for quantifying the Hsp104-GFP–labeled protein aggregates inherited by developing appressoria (left panel) and plots showing the mean number (± SEM) of Hsp104-positive aggregates inherited into developing appressoria after heat shock. For both strains and for all time points, $n > 20$. (C) Percentage of wild-type and Hsp104^{DWB} appressoria, from control and heat-shocked (HS) conidia, that contain Sep5-RFP–labeled septin rings. Data points represent independent biological replicates, where $n \geq 15$ appressoria. Error bars show the mean ± SEM from the three replicates. Asterisks indicate significance by two-way analysis of variance (ANOVA) with Tukey's multiple comparisons test (*$P < 0.05$, **$P < 0.01$, ***$P < 0.001$, ****$P < 0.0001$). (D) Time course showing the localization of Hsp104-GFP (top panel) and Hsp104^{DWB}-GFP (bottom panel) relative to the septin protein Sep5-RFP following heat shock. Images represent maximum-intensity projections of Z series acquired at 0.2 µm intervals spanning the depth of the appressoria. Scale bar = 10 µm. (E) Representative images of rice leaves of susceptible cultivar CO-39, 5 d after inoculation with conidia from wild type or Hsp104^{DWB} mutants. Leaves were either heat shocked 0.5 hpi (Early HS) or 16 hpi (Late HS) or not heat shocked (CTRL). Dark spots are necrotic lesions at inoculation sites, associated with rice blast disease. Mock infections represent water-only negative controls. (F) Plots showing the size (mm^2) of necrotic lesions/flecks emerging from leaves infected with wild type or Hsp104^{DWB} mutants under each condition. Data points represent individual lesions, and error bars show the mean lesion size (± SEM). Asterisks indicate significance by one-way ANOVA with Tukey's multiple comparisons test (*$P < 0.05$, **$P < 0.01$, ***$P < 0.001$, ****$P < 0.0001$).

certain number of aggregates (25 ± 3) migrated from the conidia into developing appressoria (Figure 3, A and D), likely as a result of bulk cytoplasmic flow (Supplemental Movie S1). These protein aggregates, though decreasing in number over time, persisted for more than 12 h in Hsp104^{DWB} mutants (Figure 3, B and D, bottom panels). In contrast, protein aggregates resolved fully within wild-type conidia, and thus their appressoria never inherited protein aggregates (Figure 3, B and D, top panels). Between 3 and 6 hpi, a septum is deposited at the neck of the appressorium, sealing off the infection cell from the germ tube and conidium (Figure 3A). While necessary for normal appressorium morphogenesis (Saunders *et al.*, 2010b), this event prevents the movement of aggregates back out of the appressorium and restricts the flow of cytoplasm into it. We wondered whether there was a penalty associated with the impaired resolution of protein aggregates and their inheritance into incipient appressoria. To test this idea, we monitored the development of appressoria from both heat-shocked and control conidia of the wild type and Hsp104^{DWB} mutant every 6 h for a total of 24 h. As a metric for appressorium maturation, we determined the time point at which Sep5-RFP (red fluorescent protein)-labeled septin rings could be observed at the base of the appressoria (Figure 3, C and D). We discovered that appressoria forming from the heat-shocked conidia of the Hsp104^{DWB} mutant lagged developmentally behind

those of heat-shocked wild-type conidia and control Hsp104^{DWB} conidia, but ultimately reached full maturation within 24 h (Figure 3C). Consistent with this observation, Hsp104^{DWB} mutants caused wild type–sized lesions on rice leaves, indicative of normal appressorium function, irrespective of heat-shock treatment (Figure 3, E and F). Thus, the impaired disaggregation of protein aggregates results in a short-term delay in appressorium morphogenesis by *M. oryzae*.

Next, we sought to investigate the ultimate cellular fate of quality control compartments that form within conidia of Hsp104^{DWB} mutants following proteostatic stress. Given that *M. oryzae* conidia undergo a type of autophagic programmed cell death, essential for appressorium function (Veneault-Fourrey *et al.*, 2006), we wondered whether these quality control compartments might too be processed by autophagy. To test this idea, we followed the fate of Hsp104^{DWB}-GFP–labeled protein aggregates relative to nuclei, which are typically degraded within the conidium around 12 hpi by nonselective macroautophagy (He *et al.*, 2012). Simultaneous imaging of Hsp-104^{DWB}-positive quality control compartments and nuclei revealed their close spatial association within conidia (Supplemental Figure S2A and Supplemental Movie S1). Furthermore, in four-dimensional time-lapse sequences these compartments appeared to undergo autophagic degradation together with nuclei (Supplemental Figure S2A and Supplemental Movie S1). Consistent with this idea, in mammalian cells lines, aggresome-containing amyloidogenic proteins are processed by autophagy (Su *et al.*, 2011; Hyttinen *et al.*, 2014), which itself can be modulated by heat shock (Dokladny *et al.*, 2015; Kumsta *et al.*, 2017). We wondered whether heat shock increases the level of autophagy within conidia, thereby promoting the degradation of protein aggregates by either selective aggrephagy (Rogov *et al.*, 2014) or nonselective bulk autophagy during infection-related development. To test this idea, we counted the GFP-Atg8–labeled autophagic puncta in non–heat-shocked and heat-shocked conidia of our Hsp104^{DWB} mutant and wild-type strain, which provides an indicator of autophagic activity (Kershaw and Talbot, 2009; Klionsky *et al.*, 2016; Supplemental Figure S2, B and C). We found that heat shock significantly increased the number of autophagic puncta in conidia of both the Hsp104^{DWB} and wild-type strain compared with controls during the first 3 h of development (Supplemental Figure S2C). However, the increased autophagic activity observed in Hsp104^{DWB} conidia was delayed compared with that of the wild-type strain (Supplemental Figure S2C), coinciding temporally with the coalescence of Hsp104^{DWB}-labeled protein aggregates (Supplemental Figure S2B).

To more directly test the role of autophagy in protein quality control during appressorium differentiation, we deleted the gene encoding the *M. oryzae* orthologue of Atg8, a small ubiquitin-like protein essential for autophagosome formation (Xie *et al.*, 2008) and autophagic cargo selection, and observed the dynamics and lifetimes of protein aggregates following heat shock (Figure 4, A–E). *M. oryzae* mutants genetically blocked in nonselective autophagy can still form appressoria, but they are unable to penetrate rice cuticles due, in part, to their inability to generate sufficiently high turgor pressure (Supplemental Figure S3A). In addition, conidia from these mutants do not undergo programmed cell death or collapse, and their organelles are not degraded and recycled (Veneault-Fourrey *et al.*, 2006; Supplemental Figure S3A). We anticipated that genetic disruption of autophagy, in combination with impaired Hsp104 disaggregase activity, would therefore result in aggregates that persisted within conidia and appressoria. When we looked at mature appressoria, we found that Hsp104/Hsp104^{DWB}-labeled protein aggregates were slower to emerge in Δ*atg8* mutant backgrounds following heat shock and had an altered, less punctate, morphology (Figure 4, D and E), possibly due to their altered biochemical and biophysical properties (Supplemental Figure S3A). As expected, in the absence of Hsp104 disaggregase, activity these structures persisted beyond 12 h in Δ*atg8* mutants, supporting a compensatory role for autophagy in aggregate clearance in differentiated appressoria (Figure 4, C and D). In striking contrast, when we looked at conidia we found that the formation of Hsp104-positive puncta within heat-shocked conidia of both our wild-type strain and Hsp104^{DWB} mutant was severely perturbed in the genetic absence of Atg8 (Figure 4, A and B) and furthermore, typical quality control compartments failed to form altogether within conidial cells (Figure 4B, see Hsp104^{DWB} panels vs. Hsp104^{DWB}Δ*atg8* panels). Besides the large reduction in aggregate number, Δ*atg8* mutants formed morphologically distinct droplet-like compartments, typically one in each cell of the three-celled conidia, that persisted beyond 12 h post–heat shock (Figure 4B). We wondered whether Atg8 might play an autophagy-independent role in the Hsp104-mediated processing of protein aggregates in *M. oryzae*, or whether this process is somehow coupled to the autophagy pathway. To investigate these ideas further, we deleted the genes encoding Atg1 (Liu *et al.*, 2007), a serine/threonine kinase required for autophagy initiation (Kamada *et al.*, 2000), and the *M. oryzae* orthologue of Cue5 (MGG_02516), an Atg8-ubiquitin adaptor required for the selective autophagic degradation of protein aggregates in budding yeast (Lu *et al.*, 2014). We found upon heat shock that the formation of Hsp104-positive protein aggregates was similarly perturbed in the genetic absence of Atg1 (Supplemental Figure S3, B and C), but not Cue5 (Supplemental Figure S3C), supporting the idea that the nonselective autophagy machinery promotes Hsp104-mediated processing of protein aggregates in our model system. Furthermore, in Δ*atg1*, but not Δ*cue5* mutants, atypical compartments emerged within conidial cells upon heat shock (Supplemental Figure S3D), consistent with those observed in the genetic absence of Atg8. Taken together, our data support an unexpected role for the autophagy machinery in the formation and spatial organization of Hsp104-labeled protein aggregates within conidial cells in response to heat shock, which is most evident when Hsp104 disaggregase activity is genetically blocked. Given this apparent interplay between autophagy and spatial protein quality control pathways in *M. oryzae*, the orthologue of the *Saccharomyce cerevisiae* aggrephagy adaptor Cue5 was surprisingly dispensable for this process.

In summary, this work provides new biological insight into the cell type–dependent control of protein homeostasis during terminal cellular differentiation by a model eukaryote and reveals a role for the autophagy machinery in the formation and compartmentalization of Hsp104-labeled protein aggregates in response to proteostatic stress. Improved mechanistic understanding of spatial protein quality control during infection-related development by *M. oryzae* may inform the development of novel control strategies for rice blast disease as well as ways to potentiate existing ones. Furthermore, new insight into the behavior of protein aggregates in terminally differentiated cell types may provide new perspective into neurodegenerative disorders where protein misfolding is pervasive.

MATERIALS AND METHODS

Fungal growth conditions

The culture and storage of *M. oryzae* were performed using standard procedures (Crawford *et al.*, 1986) and media prepared as previously described (Talbot *et al.*, 1993). Cultures were regularly maintained on complete media (CM) and incubated at 25°C under a 12:12 photoperiod for 12 d. Filter stocks were used to regenerate

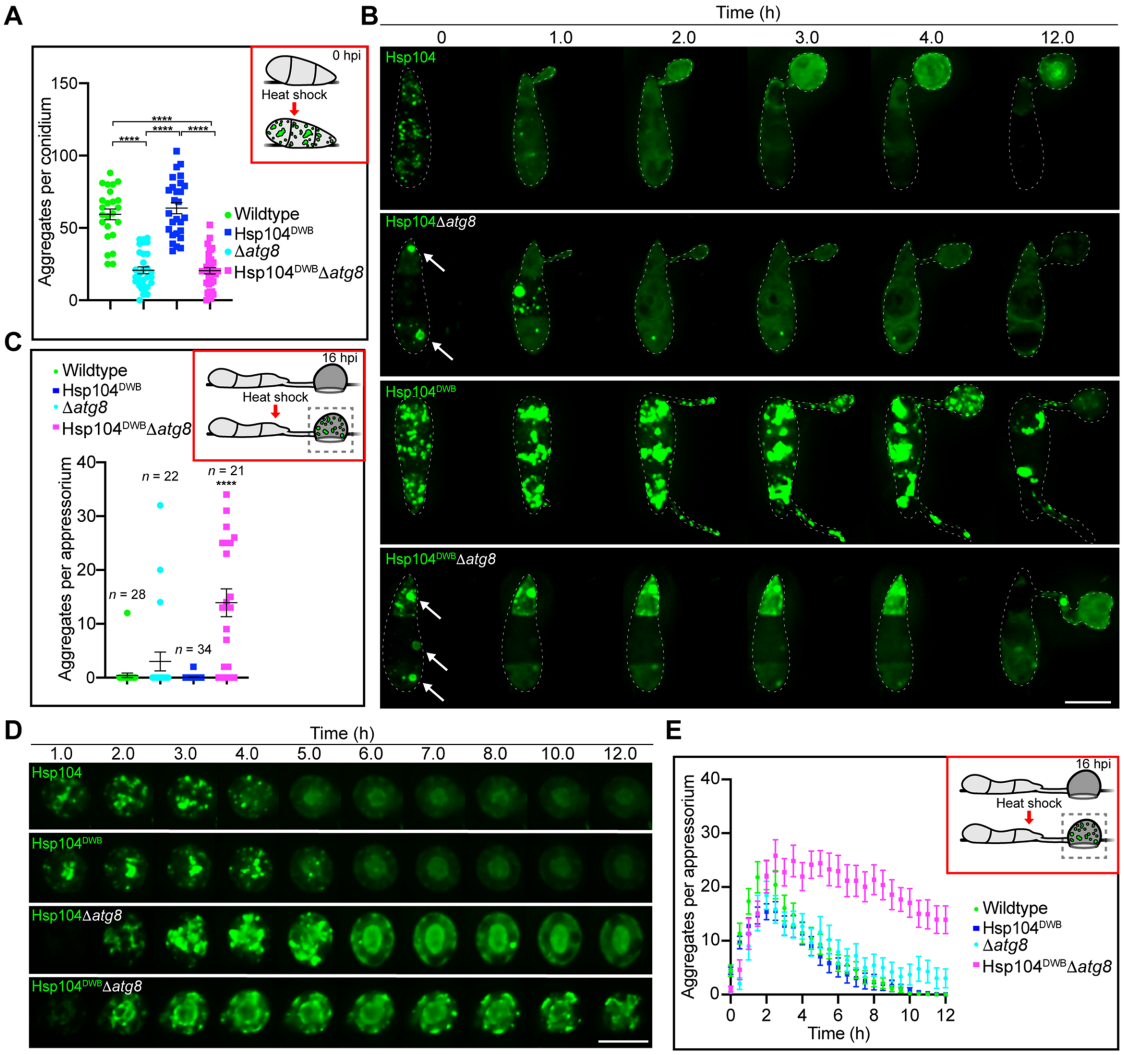

FIGURE 4: Autophagy machinery is required for normal Hsp104-mediated aggregate formation and compartmentalization. (A) Plot showing the number of Hsp104-GFP– or Hsp104^{DWB}GFP–labeled protein aggregates in wild-type or Δ*atg8* mutant conidia at 0.5 h after heat shock. Magenta lines show the mean number of aggregates/structures (± SEM). (B) Time-lapse sequences showing the localization of Hsp104-GFP– and Hsp104^{DWB}-GFP–labeled protein aggregates in wild-type or Δ*atg8* mutant backgrounds following the exposure of conidia to heat shock. White arrows highlight the presence of atypical compartments within the cells of Δ*atg8* mutants. (C) Plots showing the number of Hsp104-positive aggregates remaining in the appressoria of wild type, Hsp104^{DWB}, Δ*atg8*, and Hsp104DWBΔ*atg8* mutants after 12 h of recovery from heat shock. Error bars indicate the mean (± SEM). Asterisks indicate significance by one-way ANOVA with Tukey's multiple comparisons test (****$P < 0.0001$). (D) Time-lapse sequences showing the localization of Hsp104-GFP– and Hsp104^{DWB}-GFP–labeled protein aggregates in wild type or Δ*atg8* mutant backgrounds following the exposure of mature appressoria to heat shock. All micrographs represent maximum-intensity projections of Z series acquired at 0.2 µm intervals spanning the depth of the cells. Scale bars = 10 µm. (E) Full time course showing the mean number (± SEM) of Hsp104-positive aggregates within appressoria of wild type, Hsp104^{DWB}, Δ*atg8*, and Hsp104^{DWB}Δ*atg8* mutants, following the heat shock of mature appressoria. For wild type (Hsp104-GFP), n = 27 appressoria per time point; for Hsp104^{DWB} mutants (Hsp104^{DWB}-GFP), n = 34; for Δ*atg8* mutants, n = 22; and for Hsp104^{DWB} Δ*atg8* double mutants, n = 21. Red-boxed schematics indicate at which time point heat shock was applied.

cultures following no more than three subcultures. All strains and their genotypes used in this study are listed in Supplemental Table S1. For live cell imaging experiments, conidia were harvested from 12-d-old plates in sterile water, filtered through two layers of Miracloth (EMD Millipore), and washed twice by centrifugation (5000 × *g* for 5 min). Conidia were counted using a hemocytometer and resuspended at a concentration of 5×10^4 spores/ml in a total volume of 350 µl. Conidial suspensions were pipetted into an eight-well Nunc Lab-Tek Chambered Coverglass (Thermo Scientific) and left undisturbed for 30 min to allow the adherence of conidia to the borosilicate cover glass. Heat-shock–treated cells were then transferred to a 42°C incubator for 45 min, and imaging was initiated immediately after heat shock.

Strain construction

DNA constructs for targeted gene deletion and tagging were assembled using either In-Fusion cloning (Clontech Laboratories) or yeast gap repair (Orr-Weaver *et al.*, 1983) from linear PCR

products amplified using high-fidelity Phusion polymerase (New England Biolabs). PCR primers were designed in SnapGene (version 4.3.10; GSL Biotech), and DNA sequences were retrieved from the *M. oryzae* database (http://fungi.ensembl.org/Magnaporthe_oryzae/Info/Index). All PCR primer sequences used in this study are listed in Supplemental Table S2. To generate Hsp104-GFP and Hsp104^{DWB}-GFP fusion constructs, the *HSP104* ORF and 2 kb upstream sequence corresponding to the promoter region and 3′UTR were amplified from genomic DNA of wild-type strain Guy11 and fused in frame with a fungal codon optimized version of TagGFP2 (Egan *et al.*, 2012). The Double Walker B mutations were introduced through point mutations on primers and confirmed by sequencing. Fluorescent fusion constructs were then cloned into plasmid PCB1532, containing the *ILV1* allele conferring resistance to sulfonylurea (Sweigard *et al.*, 1997). RFP versions were generated by a one-step replacement of TagGFP2 for RFP, amplified from a Lifeact-RFP plasmid (Berepiki *et al.*, 2010). Similarly, Sep5-RFP fusion constructs were generated by a one-step replacement of eGFP for RFP, from Sep5-GFP fusion constructs (Dagdas *et al.*, 2012).

Image acquisition and analysis

Images were collected using a 100× 1.49 N.A. oil immersion Apo TIRF Nikon objective on an inverted Nikon Ti-E Eclipse epifluorescence microscope equipped with Perfect Focus System (Nikon), an iXon Ultra 897 electron multiplier charge-coupled device camera (Andor Technology), and an AURA II solid state triggered illuminator with four channel light source (395, 485, 560, 640 nm), all controlled by NIS-Elements AR (version 4.60). Data sets were deconvolved in NIS-Elements AR with spherical aberration correction and background subtraction, using the "Automatic" three-dimensional (3D) deconvolution option. Brightness and contrast adjustments to maximum-intensity projections of deconvolved 3D images were made using ImageJ (version 2.0; National Institutes of Health) and Photoshop CC (2017.1.4; Adobe), and figures were compiled in Illustrator CC (22.1; Adobe).

For comparative time-course experiments, up to four strains/conditions were imaged together using multiwell Labtek chambers (Thermo Fisher, Pittsburgh, PA). Depending on the experiment and time resolution, up to 20 conidia/appressoria per strain/condition (20 *xy* positions) were imaged at ~70 *z* positions (14 µm depth, 0.2 µm Z step).

Aggregates were automatically detected, and their number quantified over time from 4D data sets using the "spots" function in Imaris (9.3.0; Bitplane). Aggregate detection parameters were optimized with wild-type data sets, using background subtraction, an estimated *XY* diameter of 0.25 µm, and manual adjustment of the "Quality" filter. Optimized "spot" detection parameters were stored and applied to all comparative data sets. Outputs were manually inspected and refined where appropriate.

Nucleic acid isolations and analysis

Nucleic acid extraction was performed using standard cetyl trimethyl ammonium bromide (CTAB) extraction techniques as previously described (Talbot and Talbot, 2001). Subsequent PCR, gel electrophoresis, and restriction enzyme digests were carried out under standard procedures (Sambrook and Russell, 2001). DNA purification was performed using the Wizard SV Gel and PCR Clean-up System (Promega), and plasmid purification was performed using the Wizard Plus SV Minipreps DNA Purification System (Promega).

Fungal transformation

Fungal transformation was carried out on protoplasts using an established protocol (Talbot and Talbot, 2001). To generate strains expressing Hsp104-GFP and Hsp104^{DWB}-GFP, we first deleted the endogenous copy of *HSP104* by replacement with a selectable marker conferring resistance to hygromycin B, using a split marker approach (Catlett *et al.*, 2003). Replacement of the HSP104 open reading frame with the hygromycin cassette was confirmed by diagnostic PCR. The Δ*hsp104* mutant was subsequently transformed with plasmids containing either the Hsp104-GFP or Hsp104^{DWB}-GFP fusion sequence, and transformants were selected for based on resistance to sulfonylurea, conferred by an *ILV1* allele on the pCB1532 plasmid backbone (Sweigard *et al.*, 1997). The *ATG8*, *ATG1*, and *CUE5* open reading frames were replaced from both the Hsp104-GFP and Hsp104^{DWB}-GFP–expressing strains with a cassette conferring resistance to phosphinothricin and confirmed by diagnostic PCR. The Hsp104-GFP and Hsp104^{DWB}-GFP strains were transformed with plasmids containing either a Lifeact-RFP (Berepiki *et al.*, 2010; Dagdas *et al.*, 2012), a Sep5-RFP, or a Histone H1-RFP (Saunders *et al.*, 2010a), and transformants were selected based on resistance to phosphinothricin, conferred by a bar cassette on the backbone of pCB1530 (Sweigard *et al.*, 1997). To generate GFP-Atg8:Hsp104-RFP and GFP-Atg8:Hsp104^{DWB}-RFP strains, the Δ*hsp104* mutant was first transformed with a plasmid containing a GFP-atg8 fusion sequence (Kershaw and Talbot, 2009), and transformants selected based on resistance to phosphinothricin. Plasmids containing Hsp104-RFP and Hsp104^{DWB}-RFP fusion sequences were then transformed into the Δ*hsp104*;GFP-Atg8 strain, and transformants were selected based on resistance to sulfonylurea, conferred by an *ILV1* allele on the pCB1530 plasmid backbone (Sweigard *et al.*, 1997).

Plant infection assays

Three-week-old seedlings of rice (*Oryza sativa*) cultivar CO-39 were used for plant infection assays. Conidia from 12-d-old plates were harvested in a 0.2% gelatin solution, filtered through two layers of MiraCloth (EMD Millipore), and washed twice by centrifugation (5000 × *g* for 5 min). Spore concentration was determined via hemocytometer and normalized to 1×10^5 spores/ml. Fully expanded rice leaves were cut and trimmed to approximately 6 cm and immediately placed on 1.75% water agar in 100 × 15 mm sterile Petri dishes. Each leaf was inoculated with 5 × 20 µl droplets of spore suspension or 0.2% gelatin negative control. Early heat-shock–treated conidia were inoculated onto leaves, incubated at room temperature for 30 min to allow their adherence to the leaf surface, and then placed in a 42°C incubator for 45 min. Late heat-shock–treated cells were inoculated onto leaves and allowed to incubate at room temperature for 16 h before being placed in a 42°C incubator for 45 min. Leaves were imaged 5 d postinoculation on a high-resolution Epson Expression 10000XL Scanner (Epson America, Long Beach, CA).

ACKNOWLEDGMENTS

We thank Nick Talbot and Lauren Ryder for sharing GFP-Atg8, Lifeact-RFP, Sep5-GFP, and HH1-RFP plasmids and Yasin Dagdas for helpful suggestions on the manuscript.

REFERENCES

Aguilaniu H, Gustafsson L, Rigoulet M, Nyström T (2003). Asymmetric inheritance of oxidatively damaged proteins during cytokinesis. Science 299, 1751–1753.

Berepiki A, Lichius A, Shoji J-Y, Tilsner J, Read ND (2010). F-actin dynamics in Neurospora crassa. Eukaryot Cell 9, 547–557.

Catlett NL, Lee B-N, Yoder OC, Turgeon BG (2003). Split-marker recombination for efficient targeted deletion of fungal genes. Fungal Genet Rep 50, 9–11.

Chen CR, Makhatadze GI (2017). Molecular determinant of the effects of hydrostatic pressure on protein folding stability. Nat Commun 8, 14561–14569.

Crawford MS, Chumley FG, Weaver CG, Valent B (1986). Characterization of the heterokaryotic and vegetative diploid phases of Magnaporthe grisea. Genetics 114, 1111–1129.
Dagdas YF, Yoshino K, Dagdas G, Ryder LS, Bielska E, Steinberg G, Talbot NJ (2012). Septin-mediated plant cell invasion by the rice blast fungus, Magnaporthe oryzae. Science 336, 1590–1595.
de Jong JC, McCormack BJ, Smirnoff N, Talbot NJ (1997). Glycerol generates turgor in rice blast. Nature 389, 244.
Dokladny K, Myers OB, Moseley PL (2015). Heat shock response and autophagy—cooperation and control. Autophagy 11, 200–213.
Dulal N, Rogers A, Wang Y, Egan M (2020). Dynamic assembly of a higher-order septin structure during appressorium morphogenesis by the rice blast fungus. Fungal Genet Biol 140, 103385.
Egan MJ, Tan K, Reck-Peterson SL (2012). Lis1 is an initiation factor for dynein-driven organelle transport. J Cell Biol 197, 971–982.
He M, Kershaw MJ, Soanes DM, Xia Y, Talbot NJ (2012). Infection-associated nuclear degeneration in the rice blast fungus Magnaporthe oryzae requires non-selective macro-autophagy. PLoS One 7, e33270.
Hodson S, Marshall JJT, Burston SG (2012). Mapping the road to recovery: the ClpB/Hsp104 molecular chaperone. J Struct Biol 179, 161–171.
Howard RJ, Ferrari MA, Roach DH, Money NP (1991). Penetration of hard substrates by a fungus employing enormous turgor pressures. Proc Natl Acad Sci USA 88, 11281–11284.
Hyttinen JMT, Amadio M, Viiri J, Pascale A, Salminen A, Kaarniranta K (2014). Clearance of misfolded and aggregated proteins by aggrephagy and implications for aggregation diseases. Ageing Res Rev 18, 16–28.
Kaganovich D, Kopito R, Frydman J (2008). Misfolded proteins partition between two distinct quality control compartments. Nature 454, 1088–1095.
Kamada Y, Funakoshi T, Shintani T, Nagano K, Ohsumi M, Ohsumi Y (2000). Tor-mediated induction of autophagy via an Apg1 protein kinase complex. J Cell Biol 150, 1507–1513.
Kershaw MJ, Talbot NJ (2009). Genome-wide functional analysis reveals that infection-associated fungal autophagy is necessary for rice blast disease. Proc Natl Acad Sci USA 106, 15967–15972.
Klionsky DJ, Abdelmohsen K, Abe A, Abedin MJ, Abeliovich H, Arozena AA, Adachi H, Adams CM, Adams PD, Adeli K (2016). Guidelines for the use and interpretation of assays for monitoring autophagy (3rd edition). Autophagy 12, 1–222.
Kumsta C, Chang JT, Schmalz J, Hansen M (2017). Hormetic heat stress and HSF-1 induce autophagy to improve survival and proteostasis in C. elegans. Nat Commun 8, 14337.
Liu X-H, Lu J-P, Zhang L, Dong B, Min H, Lin F-C (2007). Involvement of a Magnaporthe grisea serine/threonine kinase gene, MgATG1, in appressorium turgor and pathogenesis. Eukaryot Cell 6, 997–1005.
Lu K, Psakhye I, Jentsch S (2014). Autophagic clearance of polyQ proteins mediated by ubiquitin-Atg8 adaptors of the conserved CUET protein family. Cell 158, 549–563.
Ogrodnik M, Salmonowicz H, Brown R, Turkowska J, Średniawa W, Pattabiraman S, Amen T, Abraham AC, Eichler N, Lyakhovetsky R (2014). Dynamic JUNQ inclusion bodies are asymmetrically inherited in mammalian cell lines through the asymmetric partitioning of vimentin. Proc Natl Acad Sci USA 111, 8049–8054.
Orr-Weaver TL, Szostak JW, Rothstein RJ (1983). Genetic applications of yeast transformation with linear and gapped plasmids. Methods Enzymol 101, 228–245.
Rogov V, Dötsch V, Johansen T, Kirkin V (2014). Interactions between autophagy receptors and ubiquitin-like proteins form the molecular basis for selective autophagy. Mol Cell 53, 167–178.
Sambrook J, Russell DW (2001). Molecular Cloning: A Laboratory Manual, 3rd ed., Spring Harbor, NY: Cold Spring Harbor Laboratory Press.
Saunders DGO, Aves SJ, Talbot NJ (2010a). Cell cycle–mediated regulation of plant infection by the rice blast fungus. Plant Cell 22, 497–507.
Saunders DGO, Dagdas YF, Talbot NJ (2010b). Spatial uncoupling of mitosis and cytokinesis during appressorium-mediated plant infection by the rice blast fungus Magnaporthe oryzae. Plant Cell 22, 2417–2428.
Skamnioti P, Gurr SJ (2009). Against the grain: safeguarding rice from rice blast disease. Trends Biotechnol 27, 141–150.
Sontag EM, Samant RS, Frydman J (2017). Mechanisms and functions of spatial protein quality control. Annu Rev Biochem 86, 97–122.
Spokoini R, Moldavski O, Nahmias Y, England JL, Schuldiner M, Kaganovich D (2012). Confinement to organelle-associated inclusion structures mediates asymmetric inheritance of aggregated protein in budding yeast. Cell Rep 2, 738–747.
Street TO, Bolen DW, Rose GD (2006). A molecular mechanism for osmolyte-induced protein stability. Proc Natl Acad Sci USA 103, 13997–14002.
Su M, Shi J-J, Yang Y-P, Li J, Zhang Y-L, Chen J, Hu L-F, Liu C-F (2011). HDAC6 regulates aggresome-autophagy degradation pathway of α-synuclein in response to MPP+-induced stress. J Neurochem 117, 112–120.
Subach OM, Gundorov IS, Yoshimura M, Subach FV, Zhang J, Grüenwald D, Souslova EA, Chudakov DM, Verkhusha VV (2008). Conversion of red fluorescent protein into a bright blue probe. Chem Biol 15, 1116–1124.
Sweigard JA, Chumley FG, Caroll FL, Valent B (1997) A series of vectors for fungal transformation. Fungal Genet Rep 44, 52–53
Talbot NJ, Ebbole DJ, Hamer JE (1993). Identification and characterization of MPG1, a gene involved in pathogenicity from the rice blast fungus Magnaporthe grisea. Plant Cell 5, 1575–1590.
Talbot NJ, Talbot N (2001). Molecular and Cellular Biology of Filamentous Fungi, Oxford, UK: Oxford University Press.
Veneault-Fourrey C, Barooah M, Egan M, Wakley G, Talbot NJ (2006). Autophagic fungal cell death is necessary for infection by the rice blast fungus. Science 312, 580–583.
Wilson RA, Talbot NJ (2009). Under pressure: investigating the biology of plant infection by Magnaporthe oryzae. Nat Rev Microbiol 7, 185–195.
Wojtaszek P (1997). Oxidative burst: an early plant response to pathogen infection. Biochem J 322, 681–692.
Xie Z, Nair U, Klionsky DJ (2008). Atg8 controls phagophore expansion during autophagosome formation. Mol Biol Cell 19, 3290–3298.
Zhou C, Slaughter BD, Unruh JR, Eldakak A, Rubinstein B, Li R (2011). Motility and segregation of Hsp104-associated protein aggregates in budding yeast. Cell 147, 1186–1196.